Eur. Phys. J. A **15**, 389–397 (2002)
DOI 10.1140/epja/i2001-10221-1

THE EUROPEAN PHYSICAL JOURNAL A

^{16}O-induced transfer reactions on ^{90}Zr

V. Jha[1], B.J. Roy[1,2,a], A. Chatterjee[1], H.S. Patel[1], B. Srinivasan[1], M.G. Betigeri[1], and H. Machner[2]

[1] Nuclear Physics Division, B. A. R. C., Mumbai-400085, India
[2] Institut für Kernphysik, Forschungszentrum Jülich, Germany

Received: 16 November 2001 / Revised version: 31 January 2002 /
Published online: 19 November 2002 –
Communicated by D. Guerreau

Abstract. Cross-section for transfer reactions ^{90}Zr(^{16}O, X) have been measured at an incident energy of 90 MeV. The angular distribution of the elastic scattering ^{90}Zr(^{16}O,^{16}O)^{90}Zr, the inelastic scattering to excited states of ^{90}Zr, the one-nucleon transfer reactions ^{90}Zr(^{16}O,^{15}N)^{91}Nb (g.s., 0.104 and 3.37 MeV states), ^{90}Zr(^{16}O,^{15}O)^{91}Zr (g.s. and 2.17 MeV state) ^{90}Zr(^{16}O,^{17}O)^{91}Zr (g.s.) and the two-nucleon transfer reactions ^{90}Zr(^{16}O,^{14}C)^{92}Mo (ground and 1st excited states) are analyzed in the coupled-reaction-channel (CRC) formalism. Starting with a double-folded real potential, the elastic-scattering angular distribution is calculated using the CRC code FRESCO. The absorptive potential is then generated through the coupling of various inelastic and transfer processes that occur at the nuclear surface. Addition of a short-range imaginary potential in the coupling scheme, whose purpose was to take into account the effect due to loss of flux in fusion channel, reproduces the measured elastic-scattering angular distribution. A good description of all the quasi-elastic data has been achieved and the absolute magnitudes are reproduced without any arbitrary normalization. The relative importance of the one-step cluster transfer of two protons *vs.* the two-step successive transfer has been studied.

PACS. 25.70.Hi Transfer reactions – 25.70.Bc Elastic and quasielastic scattering

1 Introduction

Nucleon(s) transfer between heavy ions represents an important reaction mechanism to understand 1) spectroscopic aspects and correlation effects in nuclei, 2) the transition from the quasi-elastic to the deep-inelastic regime and 3) coupling effects with other competing channels [1–3]. Transfer reactions are also a competitive tool for the production of neutron-rich nuclei and give access, with the availability of radioactive beams, to a wide field of nuclear structure studies in the far off-stability region. In view of its importance, a large amount of work has been carried out and is reported in the literature on heavy-ion transfer reactions. One of the main emphasis of all these works was to understand the reaction mechanism. The mechanism in which a large number of nucleons are transferred from projectile to target or viceversa is not well understood. The presence of a multi-step transfer involving sequential transfer, inelastic excitations prior or after the transfer etc., in addition to the usually dominant direct cluster transfer complicate the reaction mechanism. The number of such possibilities increases dramatically with the number of transferred nucleons and consequently it becomes more and more difficult to estabilish the reaction mechanism. On the experimental side, unambiguous data on multi-nucleon transfer reactions is not easily available. A good charge, mass and energy resolution and at the same time a high detection efficiency is a difficult task to achieve, especially, when both the colliding nuclei are heavy. In a series of measurements carried out by us at the 14UD pelletron accelerator facility at Mumbai, India, reactions corresponding to up to twelve-nucleon transfer have been observed. In these experiments a variety of target (^{56}Fe,^{88}Sr,^{90}Zr,^{115}In) and projectile (^{12}C,^{16}O,^{18}O) combinations was used. A good charge and mass separation up to $Z = 8$, $A = 18$ has been achieved using ΔE-E surface barrier detector telescopes. The work on ^{12}C +^{88} Sr, ^{12}C +^{115} In and ^{12}C +^{56} Fe has already been reported in our earlier communications [4–8]. The emphasis was on the understanding of the reaction mechanism aspects, in particular, the importance of one-step direct *vs.* multi-step sequential transfer and channel coupling effects amongst elastic, inelastic and transfer reactions.

In the present work, we report an analysis of various quasi-elastic processes induced in the collision of ^{16}O ions with ^{90}Zr nuclei at an incident energy of 90 MeV. The coupled-reaction-channel(CRC) formalism [9] allows one to couple all possible direct/indirect channels in a heavy-ion–induced reaction and hence the effect of channel cou-

[a] e-mail: b.roy@fz-juelich.de

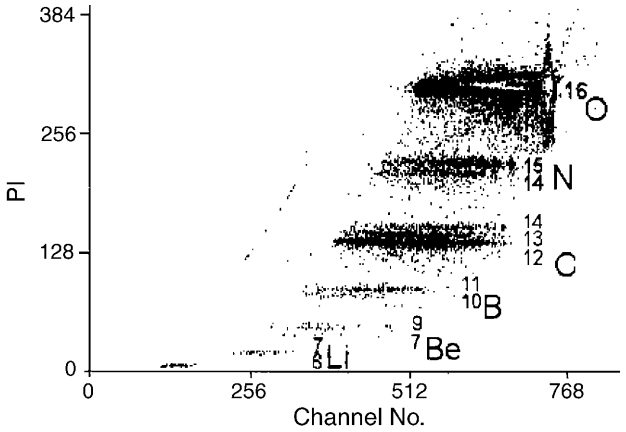

Fig. 1. Mass spectrum (PI *vs.* Energy) in ^{90}Zr(^{16}O, X) at $E_{\rm inc}$ = 90 MeV and $\theta_{\rm lab} = 30^\circ$. PI has been defined in the text.

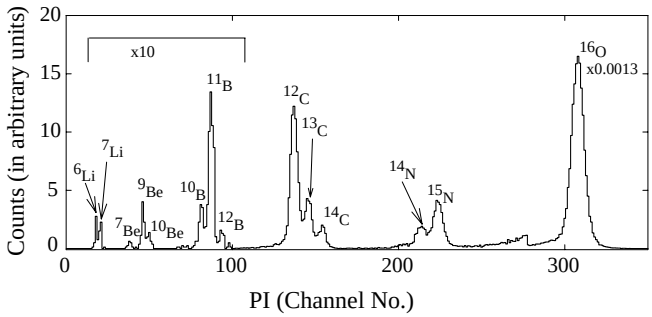

Fig. 2. Counts *vs.* PI spectrum generated from fig. 1 by taking the projection on the PI axis.

pling amongst various reaction channels and the relative importance of multi-step indirect processes as compared to the direct one-step process (for example, as in the case of two-nucleon transfer reactions, the competition between the direct cluster transfer *vs.* the two-step sequential transfer) can be studied. Single-nucleon transfer reactions are usually well described in the DWBA framework using the phenomenological optical-model potential obtained from fitting of elastic-scattering data, however, very often a large normalization factor (so-called unhappiness factor) is invoked to reproduce the absolute magnitude of the experimental cross-section. The situation in the two-proton transfer reactions is even worse. Normalization factors as large as 1000 are used to obtain agreement between experiment and one-step DWBA calculations for the (^{16}O,^{14}C) reaction [10–12]. The discrepancy improves when the successive two-step processes are included in the calculations, even then the disagreement between theory and experiment is large [11,12]. In the present work, data have been analyzed in the coupled-reaction-channel formalism with an optical potential which consisted of a bare double-folded potential for the real part and an imaginary part generated from channel couplings [13]. A consistent description of all the measured quasi-elastic data has been achieved and the magnitudes are reproduced without any arbitrary normalization. The experimental procedure is described in sect. 2, while the details of the CRC analysis of elastic, inelastic and transfer reactions are described in sect. 3.

2 Experimental procedure

Experiments are performed with ^{16}O ions of 90 MeV energy from the 14UD Pelletron accelerator in Mumbai. The targets used are isotopically enriched ($\geq$ 99 %) self-supporting ^{90}Zr of 400 μg/cm^2 thickness. Reaction products are detected using Silicon surface barrier detector telescopes (ΔE = 30 μm and E = 300 μm) mounted on two movable arms inside a 1 m diameter scattering chamber. A fast-slow coincidence set-up was employed to achieve charge and mass separation of the reaction products. Proper gain matching in ΔE and E signals led to a energy resolution of 600 keV for the elastically scattered particles. Particle identification (PI) spectrum was constructed from the measured ΔE-E plot using the familiar algorithm

$$PI = [(E + \Delta E)^n - E^n] \propto M^{n-1}Z^2$$

and the best separation is obtained with n = 1.86. It has been possible to separate and identify not only the charge but also mass separation of all the projectile-like fragments ^{6}Li to ^{16}O (figs. 1 and 2). The Q-integrated cross-section for various reaction channels has been obtained by selecting appropriate charge and mass in the PI spectrum and are listed in table 1. The errors shown in the table are statistical errors. In addition, an overall systematic uncertainty of 10% is estimated.

Various discrete transitions in the inelastic, one-nucleon and two-nucleon transfer reactions are identified. The corresponding energy spectra are shown in fig. 3. The angular distributions have been measured in the angular range $\theta_{\rm lab} = 12^\circ$ to 65°.

Table 1. Measured differential cross-section for various reaction channels in ^{16}O + ^{90}Zr at 90.0 MeV and $\theta_{\rm lab} = 20^\circ$. The differential cross-sections listed here are for the excitation energy integrated data. The reaction Q values (Q_0) listed in the table are ground-state Q values.

Reaction	Q_0 (MeV)	dσ/dΩ (mb/sr)
^{90}Zr(^{16}O,^{15}N)	−6.948	15.76 ± 0.32
^{90}Zr(^{16}O,^{14}N)	−9.915	7.550 ± 0.63
^{90}Zr(^{16}O,^{13}N)	−11.642	1.326 ± 0.09
^{90}Zr(^{16}O,^{14}C)	−9.718	5.822 ± 0.20
^{90}Zr(^{16}O,^{13}C)	−9.827	13.872 ± 0.30
^{90}Zr(^{16}O,^{12}C)	−5.094	37.825± 0.51
^{90}Zr(^{16}O,^{12}B)	−22.718	0.250± 0.04
^{90}Zr(^{16}O,^{11}B)	−16.157	2.650 ± 0.13
^{90}Zr(^{16}O,^{10}B)	−19.734	0.682 ± 0.07
^{90}Zr(^{16}O,^{10}Be)	−19.484	0.142± 0.03
^{90}Zr(^{16}O,^{9}Be)	−18.741	0.472 ± 0.06
^{90}Zr(^{16}O,^{7}Be)	−21.658	0.092 ± 0.03
^{90}Zr(^{16}O,^{7}Li)	−22.865	0.234± 0.04
^{90}Zr(^{16}O,^{6}Li)	−22.002	0.224 ± 0.04

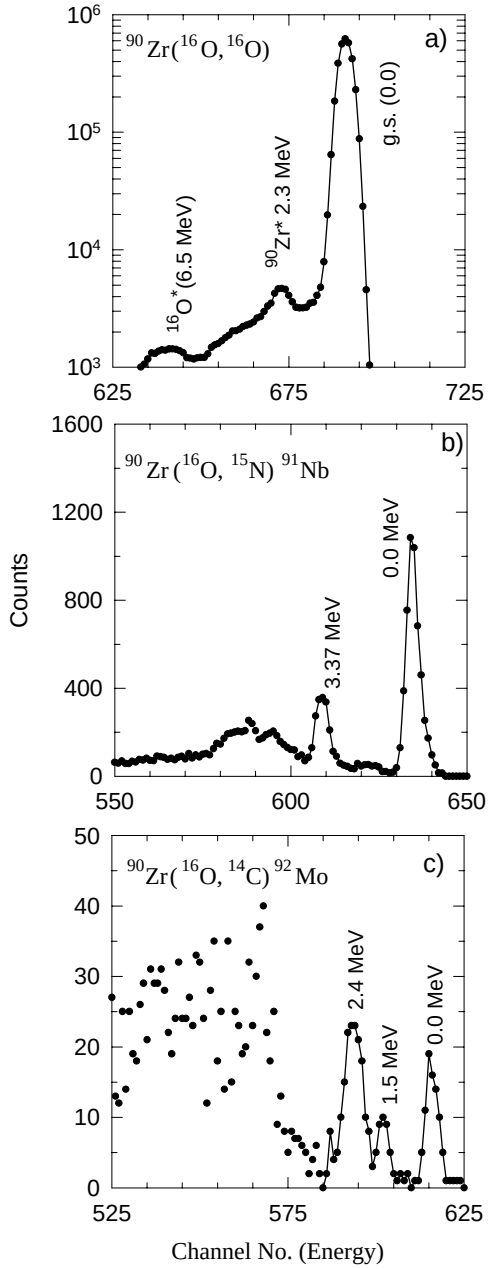

Fig. 3. Energy spectrum of a) ^{16}O from the ^{90}Zr(^{16}O, ^{16}O)^{90}Zr reaction, b) ^{15}N from the ^{90}Zr(^{16}O, ^{15}N)^{91}Nb reaction and c) ^{14}C from the ^{90}Zr(^{16}O, ^{14}C)^{92}Mo reaction all measured at an incident energy of 90 MeV and $\theta_{\rm lab} = 30^\circ$.

3 Coupled-reaction-channel calculations of ^{90}Zr(^{16}O, X)

The measured angular distributions of elastic and inelastic scattering, one- and two- nucleon transfer reactions have been analyzed in the coupled-reaction-channels (CRC) model. The computer code FRESCO (version FRX) of I. J. Thompson [9] is used. The following channels (experimentally observed strongly populated discrete transitions) are included in the coupling scheme:

i) elastic scattering ^{90}Zr(^{16}O,^{16}O)^{90}Zr,

ii) inelastic scattering for transitions to 2.18 MeV(2^+), 2.319 MeV(5^-), 2.747 MeV(3^-) excited states of ^{90}Zr and 6.14 MeV(3^-), 6.92 MeV(2^+) excited states of ^{16}O,

iii) one-proton stripping reactions ^{90}Zr(^{16}O,^{15}N)^{91}Nb (g.s., 0.104 MeV and 3.37 MeV states),

iv) two strong transitions in the $1n$ stripping reaction ^{90}Zr(^{16}O,^{15}O)^{91}Zr (g.s. and $E_x = 2.17$ MeV state),

v) the strongest transition in the $1n$ pick-up channel ^{90}Zr(^{16}O,^{17}O)^{89}Zr (g.s. $9/2^+$),

vi) two-proton stripping reactions ^{90}Zr(^{16}O,^{14}C)^{92}Mo (g.s. and 1.5 MeV 2^+ states). The relatively broad peak seen at 2.4 MeV excitation in ^{92}Mo (fig. 3) was not included in the present analysis as a number of levels exist at this excitation energy and it was not possible, within the present energy resolution, to separate and identify individual transitions.

The CRC calculations are performed as detailed below. First, the elastic-scattering angular distribution is calculated with a bare, double-folded (DF) real potential. The DF potential $V_{\rm DF} = \int\int {\rm d}\mathbf{r}_1 {\rm d}\mathbf{r}_2 \rho(\mathbf{r}_1)\rho(\mathbf{r}_2)v(\mathbf{r}_{12})$ was computed using the computer program DFPOT [14] with M3Y form of the effective nucleon-nucleon interaction $v(r_{12}) = 7999\frac{e^{-4r}}{4r} - 2134\frac{e^{-2.5r}}{2.5r} - 262\delta(r)$ and the charge densities, ρ's, taken from the atomic and nuclear data tables [15]. Next, various nonelastic modes which occur at the nuclear surface *e.g.*, inelastic and transfer processes are coupled. The absorptive potential is then generated through this coupling. The deformation parameters(δ_λ) for ^{16}O and ^{90}Zr nuclei, used in the present calculations, are taken from the experimentally extracted values reported in the literature [16,17]. The values are listed along with references in table 2. The Coulomb and nuclear deformation parameters are taken as equal. The one- and two-nucleon spectroscopic amplitudes needed for generating strengths of the various transfer processes mentioned above are taken from the data available in the literature [11,18–22]. The amplitudes along with references are listed in table 3. The two-proton transfer channel includes a one-step direct transfer as well as a two-step sequential transfer through various intermediate states as detailed in the coupling diagrams (fig. 4). The higher-order multistep transfer processes involving inelastic excitation in the target and (or) residual nuclei are not included. These effects, as also argued in ref. [11], are expected to be less significant because of the relatively small deformation parameters involved. The details of the $2p$ transfer calculations are discussed later. Finally, a short-range imaginary potential of Woods-Saxon squared shape with depth $V_0 = 50$ MeV, radius parameter $r_0 = 1$ fm and diffuseness parameter $a_0 = 0.4$ fm was added in the coupling scheme. The purpose of this imaginary potential was to take into account the effect due to the loss of flux in the fusion channel [23]. A cross-section of 1259 mb for the fusion channel has been obtained from the present calculation and the value is 1202 mb when inelastic and transfer channels are decoupled. It is to mention that no experimental fusion cross-section, to the best of our knowledge, is available for this system near the present bombarding energy. The

Table 2. Deformation lengths δ_λ and Coulomb deformation parameters of the ^{16}O and ^{90}Zr nuclei used in the calculation.

Nuclei	E_x (MeV)	J^π	Multipolarity λ	δ_λ (fm)	β_c	Ref.
^{16}O	6.13	3^-	3	1.41	0.56	[16]
	6.92	2^+	2	0.95	0.38	
^{90}Zr	2.186	2^+	2	0.42	0.092	[17]
	2.319	5^-	5	0.34	0.075	
	2.747	3^-	3	0.77	0.165	

Table 3. Spectroscopic amplitudes (SA) for various one- and two-nucleon transfers used in the present calculations.

	nlj	SA	Ref.
$^{16}O(0^+) \rightarrow {}^{15}N(1/2^-)$	$1p_{1/2}$	+1.4142	[11]
$^{16}O(0^+) \rightarrow {}^{15}N(3/2^-)$	$1p_{3/2}$	+2.00	[11]
$^{16}O(0^+) \rightarrow {}^{15}O(1/2^-)$	$1p_{1/2}$	+1.34	[18]
$^{16}O(0^+) \rightarrow {}^{17}O(5/2^+)$	$1d_{5/2}$	+0.9644	[19]
$^{16}O(0^+) \rightarrow {}^{14}C(0^+)$	$(1p_{1/2})^2$	+0.914	[11]
	$(1p_{3/2})^2$	+0.405	[11]
$^{15}N(1/2^-) \rightarrow {}^{14}C(0^+)$	$1p_{1/2}$	+0.9141	[11]
$^{15}N(3/2^-) \rightarrow {}^{14}C(0^+)$	$1p_{3/2}$	+0.2867	[11]
$^{90}Zr(0^+) \rightarrow {}^{91}Nb(9/2^+)$	$1g_{9/2}$	+0.9657	[11]
$^{90}Zr(0^+) \rightarrow {}^{91}Nb(1/2^-)$	$2p_{1/2}$	−0.5799	[11]
$^{90}Zr(0^+) \rightarrow {}^{91}Nb(5/2^+)$	$2d_{5/2}$	+0.5744	[20]
$^{90}Zr(0^+) \rightarrow {}^{91}Zr(5/2^+)$	$2d_{5/2}$	+0.8062	[21]
$^{90}Zr(0^+) \rightarrow {}^{91}Zr(11/2^-)$	$1h_{11/2}$	+0.7280	[21]
$^{90}Zr(0^+) \rightarrow {}^{89}Zr(9/2^+)$	$1g_{9/2}$	+0.8944	[22]
$^{90}Zr(0^+) \rightarrow {}^{92}Mo(0^+)$	$(1g_{9/2})^2$	+1.084	[11]
	$(2p_{1/2})^2$	−0.4843	[11]
$^{90}Zr(0^+) \rightarrow {}^{92}Mo(2^+)$	$(1g_{9/2})^2$	+0.9300	[11]
	$(2p_{1/2})^2$	0.0	[11]
$^{91}Nb(9/2^+) \rightarrow {}^{92}Mo(0^+)$	$1g_{9/2}$	+1.5834	[11]
$^{91}Nb(1/2^-) \rightarrow {}^{92}Mo(0^+)$	$2p_{1/2}$	+1.1809	[11]
$^{91}Nb(1/2^-) \rightarrow {}^{92}Mo(2^+)$	$1g_{9/2}$	+1.3642	[11]

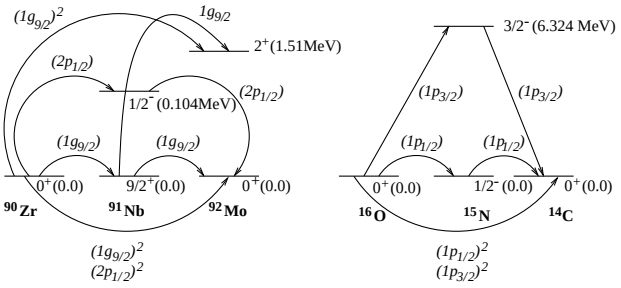

Fig. 4. Coupling diagram showing the different transfer paths used in the CRC calculations.

variation of the CRC results with the parameters of this absorptive potential is discussed at the end of this section.

The CRC results for the elastic channel are shown in fig. 5. The effects of inclusion of inelastic, transfer channels and the short-range imaginary potential are also shown. The elastic and inelastic channels are observed to be strongly coupled, in particular, the 3^- state of ^{16}O which has a relatively large deformation parameter affects

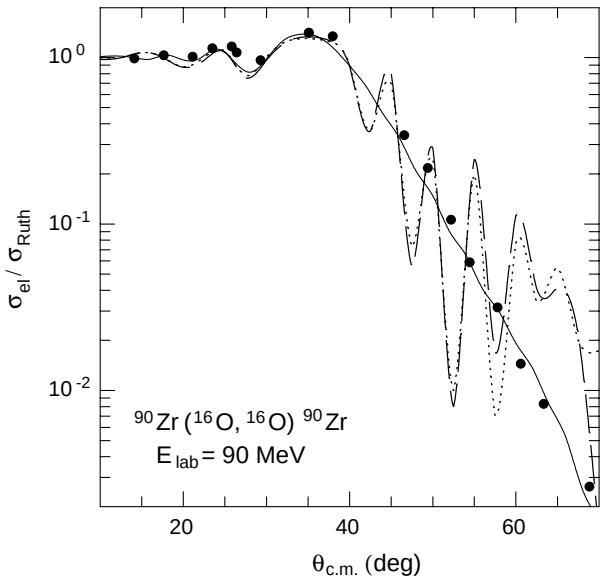

Fig. 5. Elastic-scattering angular distributions for the system ^{90}Zr + ^{16}O at $E(^{16}\text{O}) = 90$ MeV. The results of the FRESCO calculations are shown as i) dashed curves when only inelastic channels are coupled, ii) dotted curves when inelastic plus transfer coupling is considered and iii) solid line when a short-range imaginary potential was included in addition to the transfer plus inelastic coupling. See text for details.

the elastic angular distribution the most. The inclusion of transfer processes did not make any significant change in the elastic-scattering cross-section. The measured elastic-scattering angular distribution after inclusion of all the channels, as mentioned above, is well reproduced by the calculation (fig. 5). The present prescription simultaneously describes the measured inelastic and transfer angular distributions as detailed below.

The angular distributions for the one-nucleon transfer reactions ^{90}Zr(^{16}O,^{15}N) are plotted in fig. 6. The data shown in the figure (fig. 6a) include the experimentally unresolved ground and 1st excited states ($E_x = 0.104$ MeV) of ^{91}Nb. However, as calculations indicate, the maximum contribution is due to the $9/2^+$ g.s. (dotted line shown in the figure). The cross-section for the 1st excited state ($1/2^-$) (dashed line) is about one order of magnitude less than that for the ground state. The incoherent addition of these two states is also shown (solid line). In fig. 6b, the data and CRC results for the transition to the $5/2^+(E_x = 3.37$ MeV) state are displayed. All the CRC results presented here are of absolute magnitude without any arbitrary normalization factor. A reasonable good agreement between the measurement and present CRC calculations is obtained. No normalization constant (so-called unhappiness factor in standard DWBA finite-range calculations) is needed. The disagreement between the measurement and the calculation at forward angles for the g.s. transition is significant. Some refinement in the fit may be obtained by varying exit channel potential as usually followed in the literature [24,10], however, it was not done in the present study.

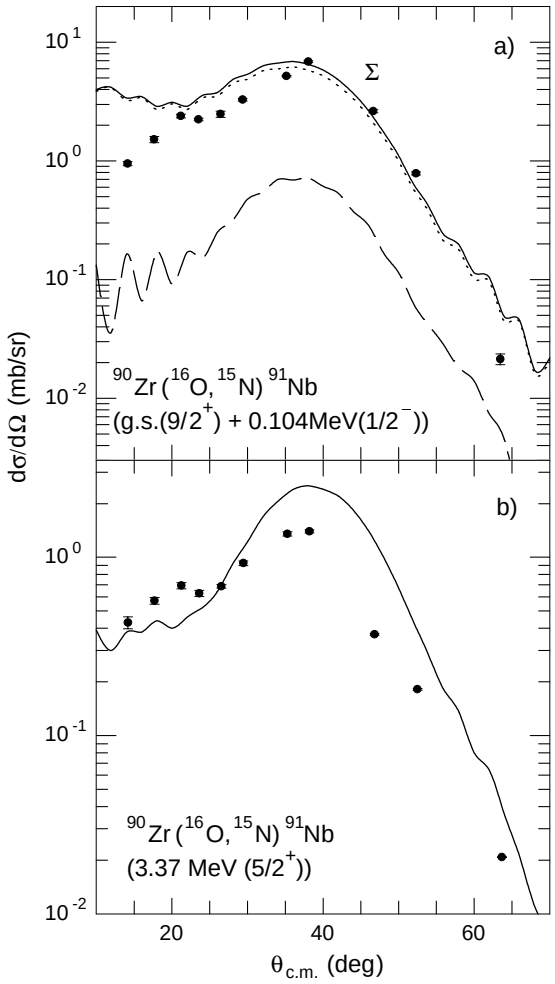

Fig. 6. Angular distribution of ^{90}Zr(^{16}O,^{15}N) in transition to the a) unresolved ground and E_x = 0.104 MeV states and b) E_x = 3.37 MeV state in ^{91}Nb. The lines drawn are the results of CRC calculations. The line represented by Σ in a) corresponds to the sum of the contribution from the two unresolved states at $E_x \approx 0$ MeV.

In fig. 7, the CRC results along with data for one-neutron transfer reactions ^{90}Zr(^{16}O,^{15}O)^{91}Zr(g.s. and E_x = 2.2 MeV) and ^{90}Zr(^{16}O,^{17}O)^{89}Zr(g.s.) are shown. A number of close-lying levels exists around the 2 MeV excitation in ^{91}Zr. In an earlier study [20] of heavy-ion–induced one-neutron stripping reaction on the same target nucleus at an incident energy close to the present one, the largest cross-section was observed due to the state at 2.17 MeV($11/2^-$). Also the peak observed in the present reaction is quite narrow with about the same FWHM as that of the g.s. The present calculations are, therefore, performed for the $11/2^-$ (2.17 MeV) state (fig. 7b). However, calculations were also repeated by including some of the close-lying states (2.04($3/2^+$), 2.13(($9/2^+$), 2.19($5/2^-$) and 2.201($7/2^+$) MeV) and the observation is that the $11/2^-$ state has the maximum contribution amongst all these. As is obvious in the figure, the $11/2^-$ state alone accounts for the observed cross-section. The absolute magnitude is also well reproduced for the g.s. transition. However, the CRC predictions in both the cases are broader than the experimental angular distributions. Finite-range DWBA calculations for the same states populated via the $1n$ stripping reaction ^{90}Zr(^{12}C,^{11}C)^{91}Zr also report a similar failure in predicting the shape of the measured angular distribution. The reason for this disagreement, as is hinted in ref. [21], could be due to a large angular-momentum mismatch between the entrance and exit channels ($L^i_{\rm gr} \approx 45\hbar$ and $L^f_{\rm gr} \approx 38\hbar$). A similar explanation may well be valid for the present reaction also ($L^i_{\rm gr} \approx 37\hbar$ and $L^f_{\rm gr} \approx 29\hbar$).

Calculations do reproduce the measured cross-section for $1n$ pick-up reaction ^{90}Zr(^{16}O, ^{17}O)^{89}Zr(g.s.). It is to mention that the peak observed at 0.0 MeV excitation energy in this channel has a long tail extending up to 2.0 MeV. A Gaussian of the same width (FWHM = 600 keV) as that observed for the g.s. transition in ^{90}Zr(^{16}O,^{15}O)^{91}Zr was fitted to extract the cross-section for the ground state of ^{89}Zr. The single-nucleon spectroscopic factors that are used in the present calculations for various transitions are listed in table 3. All single-nucleon transfer calculations presented here were performed in the prior representation of the transition potential with similar results obtained in the post representation. The transition potentials were chosen as those which are responsible for binding the nucleon to the corresponding core nuclei. A Woods-Saxon form of this potential with the following standard choice of r_0 = 1.25 fm and a_0 = 0.6 fm for the radius and diffuseness parameters was taken. The depth of the transition potentials were adjusted to reproduce the correct one-nucleon separation energy in the corresponding nuclei. The Coulomb radius parameter was assumed to be r_{0c} = 1.25 fm. It has been observed, in additional calculations, that the calculated single-nucleon transfer cross-sections, as usual, depends strongly on the geometry(r_0 and a_0) of bound states, however, the shape remains more or less the same.

In the analysis of two-proton transfer reactions, combined simultaneous (one step) and successive (two step) transfer calculations were performed with an emphasis to understand the relative importance of these two paths. The ground and 1st excited states of ^{92}Mo have been described, in the truncated ($2p_{1/2}$, $1g_{9/2}$) shell model, as [11]

$$\psi_{\rm g.s.} = -0.4843(2p_{1/2})^2 + 1.084(1g_{9/2})^2\,,$$

$$\psi_{1.51\rm MeV} = 0.93(1g_{9/2})^2\,.$$

Therefore, in the description of the sequential process for the ^{90}Zr(0^+) to ^{92}Mo(0^+) transition, two intermediate channels populating the $9/2^+$(g.s.) and $1/2^-$(1st excited state) in ^{91}Nb are considered, while the ^{90}Zr(0^+) to ^{92}Mo(2^+) transition includes one intermediate channel, $9/2^+$, of ^{91}Nb (see fig. 4). Successive calculations were treated as a two-step transfer of single nucleons where the interaction/transition potential acts twice. In each step of a sequential transfer, the appropriate measured one-proton separation energies were used in constructing the form factors. The two-step calculations were performed in the prior-post representation of the transition potential so

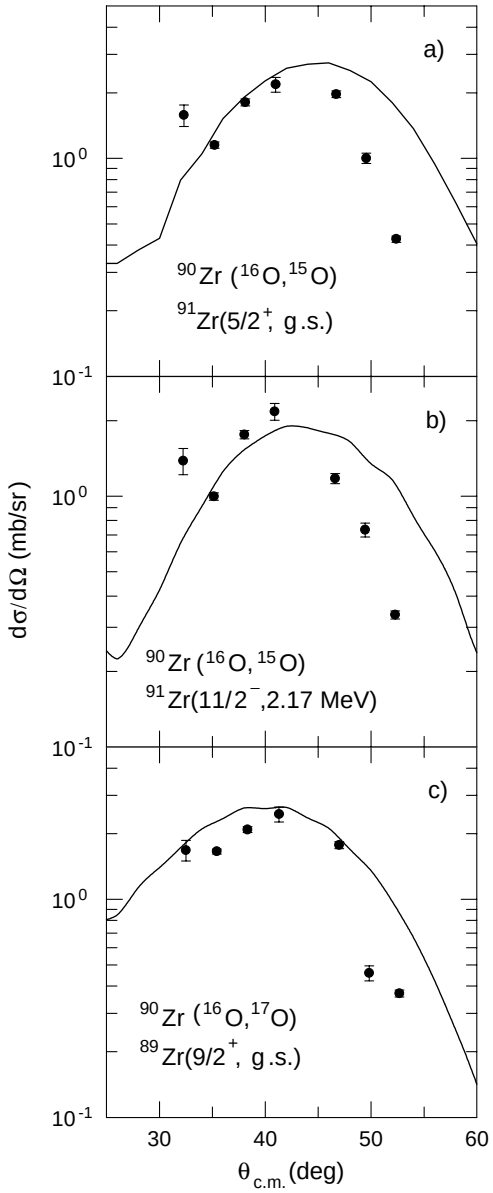

Fig. 7. Angular distribution of the $1n$ transfer reaction ^{90}Zr(^{16}O,^{15}O) in transition to a) the g.s. and b) the E_x = 2.2 MeV state in ^{91}Zr. In c), the angular distribution for the g.s. transition in the neutron pick-up reaction is displayed. Solid lines are the CRC calculations.

as to make cancellation of the so-called "non-orthogonality terms" [9,25].

For the simultaneous-transfer calculations, two approaches were followed: extreme cluster and microscopic calculations. In the extreme cluster model [25], the interaction is assumed to act on the centre of mass of the correlated proton pair and not on its internal variable. In this situation, the transfer is described in the same way as that for a single nucleon. The $2p$ cluster was assumed to be in the $S = 0$, $T = 1$ state and the $0s$ internal motion ($n = 0$, $l = 0$) for these nucleons were considered. The quantum numbers (N, L) of the centre-of-mass motion were restricted to satisfy the harmonic-oscillator energy conservation relation

$$(2N + L) + (2n + l) = \sum_{i=1,2} (2n_i + l_i)\,,$$

where $(n_i,\ l_i)$ are the quantum numbers of the individual transferred nucleons. The initial and final bound-state wave functions were calculated in a Wood Saxon potential well with $R = 1.2A^{1/3}$ fm, $a_0 = 0.60$ fm and the depth of the potential was adjusted for the two-proton separation energy. The transition potential is the same as that responsible for binding the $2p$ to the core. The post form of the transition potential was used with prior form of the potential giving similar results. Also included in the calculations are the full "remnant" terms which are due to the difference in the core-core interaction [9].

In the microscopic approach [25], where the transition potential acts separately on each of the transferred nucleons and the transfer pair is not restricted to be in a state of zero total spin and zero relative angular momentum, the form factors were generated by transforming two single-particle eigenfunctions of a Wood Saxon potential. The radius and diffuseness parameter of the well were taken as $r_0 = 1.2$ fm and $a_0 = 0.6$ fm. The depth of the potentials were adjusted to reproduce half the two-proton separation energy and the post-form of the transition potential was taken.

The CRC results along with the experimental data for the two-proton transfer reaction ^{90}Zr(^{16}O, ^{14}C)^{92}Mo (g.s.) are shown in fig. 8a. A very good agreement (both in shape and absolute magnitude) between the calculation (cluster model) and data for the present two-proton transfer reaction has been obtained. It is again to emphasize that the absolute magnitude of $2p$ cross-section is reproduced without the need for any arbitrary normalization. We also observed: i) the two-step sequential process, as shown by the dotted line in the figure, is more than one order of magnitude smaller as compared to the cluster calculation, ii) the microscopic calculations are successful in reproducing the shape of the measured angular distribution but the absolute magnitude is far off and iii) the contribution from the two-step sequential process is 6 times more than from the one-step direct process when only microscopic calculations are considered. The combined sequential plus microscopic calculation underpredicts the absolute magnitude. Similar results (point iii)) were also obtained by Tung *et al.* [11] for the same reaction studied at a relatively lower energy of 80 MeV. The relative contribution of the sequential process, in those calculations, was found to be a factor 4 larger than for the one-step transfer, and the absolute magnitude, even after the simultaneous and successive processes were combined, was nowhere close to the experimental value ($N = \sigma_{\rm exp}/\sigma_{\rm cal} = 139$ as quoted in ref. [11]).

The coupled-reaction-channel calculations for the $2^+(E_x = 1.509\,\text{MeV})$ state in ^{92}Mo (fig. 8b) reproduce the shape of the measured angular distribution very well. The absolute magnitude in the extreme cluster model when calculated with bound-state well radii $R = 1.2A^{1/3}$ fm is over-predicted but the magnitude is correctly reproduced

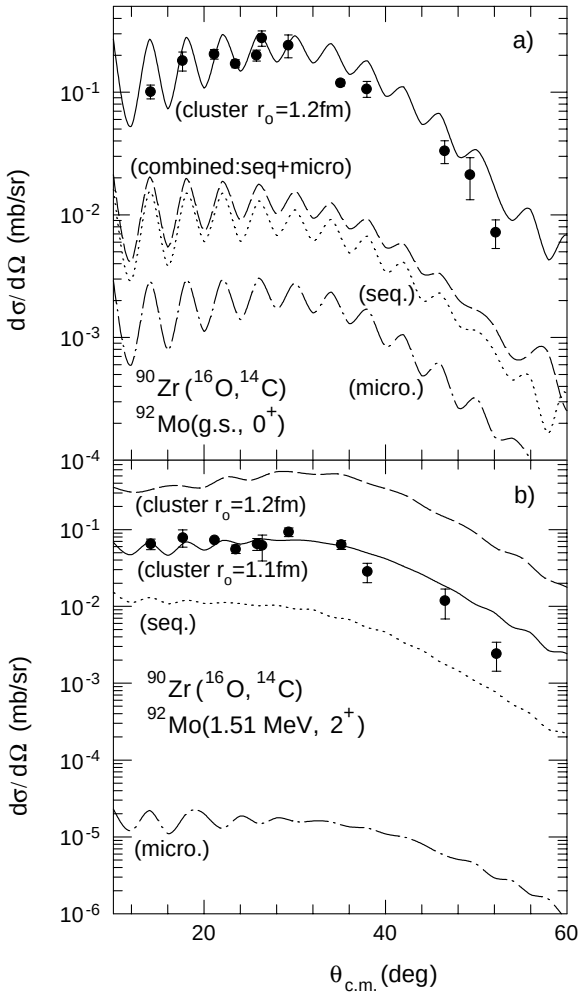

Fig. 8. Cross-section for a) the g.s.(0^+) and b) the 1.509 MeV(2^+) state of ^{92}Mo populated via the two-proton transfer reaction ^{90}Zr(^{16}O, ^{14}C) plotted as a function of $\theta_{\rm cm}$. The solid and dash dotted lines are results of CRC calculations for the simultaneous transfer using the cluster and microscopic form factor, respectively, while the dotted curve is the calculation for the two-step sequential processes. The results of the combined cluster+successive calculation are about the same as that of the cluster alone and hence they are not shown separately. The results of combined sequential+microscopic calculation for the 2^+ state merge with the dotted curve.

when the radius is changed to $R = 1.1A^{1/3}$ fm. Again, the microscopic calculations, as in the previous case, underpredict the absolute magnitude of the measured cross-section and is also much lower as compared to the results of two-step calculations.

The cluster transfer cross-section is usually very sensitive to the choice of binding well radius [25]. A small change in the binding potential can result in large changes in the cross-section. There are earlier studies reported in the literature [26,10] on two-nucleon transfer reactions where a change in the cross-section as large as a factor of 100 is observed when the radius is changed from $R = 1.2A^{1/3}$ to $R = 1.2(A^{1/3} + 2^{1/3})$ ($\approx 50\%$ change in the radius). In the present work, the effect of the bound-state radius parameter on the cluster transfer cross-section has been investigated. The results so obtained are tabulated in table 4. A change in radius from $R = 1.2A^{1/3}$ to $1.3A^{1/3}$ fm for both projectile and residual nucleus leads to an increase in the ^{92}Mo (g.s.) cross-section by a factor of ≈ 5, while the cross-section goes down by a factor of about 10 when the radius is decreased to $R = 1.1A^{1/3}$ fm. A similar variation in the cross-section (a factor of 6 increase for a change in r_0 from 1.2 to 1.3 fm and a factor of about the same decrease for a decrease in r_0 from 1.2 to 1.3 fm) is also observed for the ^{92}Mo (2^+ excited state). The shape of the angular distributions for both the transitions was observed to remain insensitive to the choice of bound-state radii. Thus, the magnitude of the two-proton cluster transfer cross-section depends very much on the choice of the radius of the cluster well potential, however, a choice of radius $R \approx 1.1A^{1/3}$ to $1.2A^{1/3}$ fm yields correct magnitude of the present $2p$ transfer cross-sections.

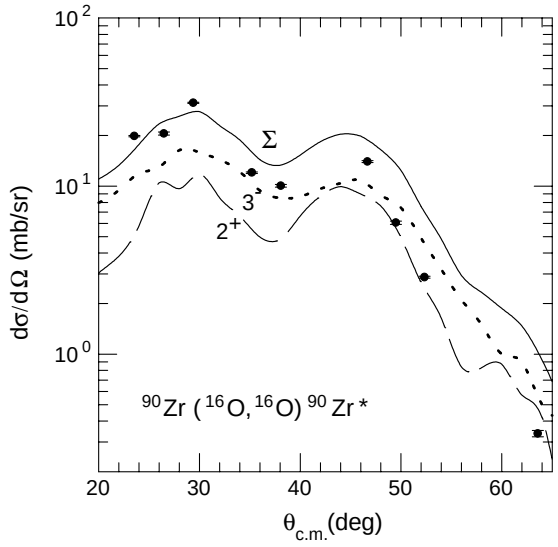

Fig. 9. Angular distribution of the inelastic scattering of ^{90}Zr(^{16}O,^{16}O)^{90}Zr*. The CRC results are represented by the long dashed curve for the 2.17 MeV (2^+) state and dotted curve for the 2.47 MeV (3^-) state. The incoherent addition of these two contributions is shown as solid line (curve labelled as Σ).

The results of the inelastic-scattering angular distribution are plotted in fig. 9. The peak seen at 2.3 MeV excitation energy in ^{90}Zr (fig. 3) is relatively broader and may include a number of states present in this excitation energy region. In a high-resolution study [21] of inelastic scattering from ^{12}C on ^{90}Zr at an incident energy (98 MeV) close to the present one, only two states (2^+ at 2.186 MeV and 3^- at 2.748 MeV) are observed to be strongly excited. The present calculations were performed for these two transitions only and the incoherent addition (solid line in fig. 9) of the contribution from these two individual transitions were used for the comparison with experimental data. However, the 5^- state at 2.32 MeV which has relatively large deformation parameter (table 2) and two states in the projectile excitation (6.14 MeV(3^-) and 6.92 MeV(2^+)) are also added in the coupling scheme in order to include their effects on the elastic as well as

Table 4. Bound-state radius dependence of $2p$ transfer cross-section in the extreme cluster model (values are at a representative point of $\theta_{\rm cm} = 20^\circ$).

^{92}Mo*	J^π	Calculated cross-section (mb/sr)		
(MeV)		$R = 1.1A^{1/3}$ fm	$R = 1.2A^1/3$ fm	$R = 1.3A^{1/3}$ fm
0.0	0^+	0.022	0.28	1.3
1.51	2^+	0.053	0.32	1.85

Table 5. Variation of CRC cross-sections (angle integrated) on the radius of the short-range absorptive potential with V_0 (= 50 MeV) and a_0 (= 0.4 fm) being fixed.

Reaction channel	CRC cross-sections (mb)		
	$r_0 = 1$ fm	$r_0 = 1.2$ fm	$r_0 = 1.4$ fm
Fusion	1259	1207	1288
^{91}Nb($9/2^+$)	11.86	14.28	6.33
($1/2^-$)	0.94	1.15	0.71
($5/2^+$)	3.63	4.47	2.90
^{91}Zr($5/2^+$)	4.44	6.48	3.98
($11/2^-$)	3.05	4.17	2.51
^{89}Zr($9/2^+$)	4.43	5.55	2.47
^{92}Mo(0^+)	0.42	0.66	0.20
(2^+)	0.72	1.13	0.43
^{90}Zr*(2^+)	11.18	11.53	14.3
(5^-)	9.62	9.71	6.91
(3^-)	22.78	23.34	18.12

Table 6. Variation of CRC cross-sections (angle integrated) on the depth of the short-range absorptive potential with r_0 (= 1 fm) and a_0 (= 0.4 fm) being fixed.

Reaction channel	CRC cross-sections (mb)		
	$V_0 = 10$ MeV	$V_0 = 50$ MeV	$V_0 = 80$ MeV
Fusion	1217	1259	1261
^{91}Nb($9/2^+$)	14.45	11.86	12.03
($1/2^-$)	1.12	0.94	0.91
($5/2^+$)	4.38	3.63	3.77
^{91}Zr($5/2^+$)	5.26	4.44	4.47
($11/2^-$)	3.62	3.05	3.07
^{89}Zr($9/2^+$)	4.89	4.43	4.46
^{92}Mo(0^+)	0.65	0.42	0.42
(2^+)	1.13	0.72	0.72
^{90}Zr*(2^+)	11.30	11.18	12.88
(5^-)	9.86	9.62	9.64
(3^-)	23.39	22.78	23.05

other channels. The data are satisfactorily described by the calculations. Both the 2^+ and 3^- states have comparable strength, while the 5^- state is observed to be less in magnitude.

The sensitivity of the present CRC results to the short-range absorptive potential has been studied. A set of CRC calculations have been carried out in which the radius, depth and diffuseness parameters are varied. The results for angle-integrated (from 10° to 70°) cross-section are tabulated in tables 5 and 6 and our observation is as follows. When the radius is increased from $r_0 = 1$ fm to 1.2 fm, a small reduction ($\sim$ 4%) in the fusion cross-section is noticed while the transfer and inelastic cross-sections, in general, are increased. By increasing r_0 to 1.4 fm, the fusion cross-section again increases and the quasi-elastic (inelastic+transfer) cross-sections are reduced. The enhancement of fusion cross-section for an increase of r_0 from 1 to 1.4 fm has also been observed in the CRC calculation of Thomson [27] for ^{16}O + ^{208}Pb. The effect of the reduction of the depth of the potential is to reduce the fusion cross-section and to increase the quasi-elastic cross-sections while an increase of V_0 from 50 MeV to 80 MeV seems to have little effect. The effect of a_0 (diffuseness parameter) variation from 0.2 to 0.6 fm is negligible.

The α stripping has also been included in the coupling scheme in order to study its influence on other reaction channels. The experimental energy spectrum for ^{90}Zr(^{16}O, ^{12}C) has a broad peak around $Q \sim 20$ MeV and it was not possible, within the present energy resolution, to identify any discrete transition hence this channel was coupled as follwed in ref. [27]: a single α-transfer channel with a Q-value = 20 MeV and a form factor obtained by binding the α-particle on ^{90}Zr with 1 MeV binding energy. The strength was adjusted to reproduce the measured angle-integrated (from 10° to 70°) cross-section of $\sim$ 60 mb. We noticed (as shown in table 7) that coupling of α-transfer, though it accounts for a significant part of the total reaction, has a little influence on other channels (a small decrease in fusion as well as quasi-elastic cross-sections). It is to mention that Thompson [27] and also Sastry [28] have studied the effect of α-transfer for the ^{16}O + ^{208}Pb sytem at various energies and the present findings are consistent with their observations.

4 Conclusion

The angular distributions of the elastic scattering ^{90}Zr(^{16}O,^{16}O)^{90}Zr, the inelastic scattering to excited states of ^{90}Zr at $E_x = 2.3$ MeV, the one-nucleon transfer reactions ^{90}Zr(^{16}O,^{15}N)^{91}Nb ($E_x = 0$ and 3.37 MeV states), ^{90}Zr(^{16}O,^{15}O)^{91}Zr (ground and $E_x = 2.0$ MeV states), ^{90}Zr(^{16}O,^{17}O)^{89}Zr (g.s.), and the two-nucleon transfer reactions ^{90}Zr(^{16}O, ^{14}C)^{92}Mo (ground and 1st excited states) have been measured at an incident energy of $E(^{16}\text{O}) = 90$ MeV. Coupled-reaction-channel calculations with full recoil and exact finite-range couplings using the code FRESCO [9] have been performed by coupling all these quasi-elastic transitions. In addition, a short-range absorptive potential was included. The interaction potential, thus generated by the CRC calcu-

Table 7. Angle-integrated cross-section in mb.

Cross-section	Couplings in the CRC calculations	
	without α coupling	with α coupling
Fusion	1259	1224
^{91}Nb$(9/2^+)$	11.86	13.25
$(1/2^-)$	0.94	0.91
$(5/2^+)$	3.63	3.4
^{91}Zr$(5/2^+)$	4.44	3.25
$(11/2^-)$	3.05	2.43
^{89}Zr$(9/2^+)$	4.43	3.95
^{92}Mo(0^+)	0.42	0.43
(2^+)	0.72	0.72
^{90}Zr$^*(2^+)$	11.18	10.77
(5^-)	9.62	8.21
(3^-)	22.78	13.15

lations in this coupling scheme, is successful in describing the quasi-elastic data. The absolute magnitudes of one-nucleon transfer cross-sections have been reproduced. This, as we have seen, obviates the necessity for introducing any arbitrary normalization constant (so-called unhappiness factor in the finite-range DWBA calculations). The combined simultaneous/successive transfer calculations have been performed for the $2p$ transfer reactions. For simultaneous transfer, calculations were performed using both the cluster form factor and the microscopic form factor. Though the shape of the measured angular distribution is well reproduced by both the calculations, the microscopic calculation underpredicts the absolute cross-section and is also much lower as compared to the two-step sequential magnitude. The two-step successive processes, usually important in heavy-ion transfer reactions, also underpredict the present $2p$ cross-sections. The simple cluster model calculation (assuming the $0s$ internal motion of the two protons), though very much depends on the bound-state well radii, reproduces correctly the magnitude of the measured $2p$ cross-sections with radius $R \approx 1.1A^{1/3}$ to $1.2A^{1/3}$ fm. The reason behind the present large discrepancy between the microscopic and cluster model results is not very clear; however, as is also mentioned in ref. [10] it is not very surprising as the two treatments calculate the two-proton form factor differently. On the other hand, such a good agreement in the present CRC calculation with cluster form factor probably indicates that the $0s$ internal representation of the $2p$ cluster is a fairly good approximation, at least, for the transitions concerned here.

The authors would like to thank the operation staff of the Pelletron Accelerator for the excellent support during the experiment. Two of the authors(VJ and BJR) are greatly indebted to Dr. B.K. Jain and Dr. S. Kailas for valuable discussions and suggestions.

References

1. Wu C.Y., Von Oertzen W., Cline D., Guidry M., Annu. Rev. Nucl. Part. Sci. **40** , 285 (1990).
2. Rehm K.E., Annu. Rev. Nucl. Part. Sci. **41**, 429 (1991). and references therein.
3. Stefanini A.M., Nebbia G., Lunardi S., Montagnoli G., Vitturi A., *Proceedings of the International Workshop on Heavy-Ion Fusion: Exploring the Variety of Nuclear Properties, 25-27 May 1994, Padova (Italy)* (World Scientific, Singapore, 1995).
4. B.J. Roy, M.G. Betigeri, H.C. Jain, M.L. Jhingan, Nucl. Phys. A **564**, 271 (1993).
5. B.J. Roy, B. Srinivasan, E. Shallom, M.G. Betigeri, H.C. Jain, M.L. Jhingan, Nucl. Phys. A **588**, 706 (1995).
6. B.J. Roy, B. Srinivasan, M.G. Betigeri, H.C. Jain, M.L. Jhingan, Nucl. Phys. A **597**, 151 (1996).
7. H.S. Patel, B. Srinivasan, B.J. Roy, M.G. Betigeri, Pramana J. Phys. **51**, 443 (1998).
8. H.S. Patel, B. Srinivasan, B.J. Roy, M.G. Betigeri, Pramana J. Phys. **53**, 843 (1999).
9. I.J. Thompson, *Computer code FRESCO (version FRX)*, Comput. Phys. Rep. **7**, 167 (1988).
10. Y. Eisen, H.T. Fortune, W. Henning, D.G. Kovar, S. Vigdor, B. Zeidman, Phys. Rev. C **13**, 699 (1976).
11. P.P. Tung, K.A. Erb, M.W. Sachs, G.B. Sherwood, R.J. Ascuitto, D.A. Bromley, Phys. Rev. C **18**, 1663 (1978).
12. R.E. Rehm, B. Glagola, W.C. Ma, W. Phillips, F.L.H. Wolfs, Z. Phys. A **340**, 281 (1991).
13. I.J. Thompson, M.A. Nagrajan, J.S. Lilley, B.R. Fulton, Phys. Lett. B **157**, 250 (1985).
14. J. Cook, *DFPOT, A computer code for calculating double folding potentials*, Comput. Phys. Commun. **25**, 125 (1982).
15. H. De Vries, C.W. De Jager, C. De Vries, At. data Nucl. data tables **36**, 495 (1987).
16. K.T. Knopfle, G.J. Wagner, H. Breuer, M. Rogge, C. Mayer-Boricke, Phys. Rev. Lett. **35**, 779 (1975).
17. M. Lahanas, D. Rychel, P. Singh, R. Gyufko, D. Kolbert, B. Van Kruchten, E. Madadakis, C.A. Weidner, Nucl. Phys. A **455**, 399 (1986).
18. J.L. Snelgrove, E. Kashy, Phys. Rev. **187**, 1246 (1969).
19. M.D. Cooper, W.F. Hornyak, P.G. Roos, Nucl. Phys. A **218**, 249 (1974).
20. M.S. Zisman, F.D. Becchetti, B.G. Harvey, D.G. Kovar, J. Mahoney, J.D. Sherman, Phys. Rev. C **8**, 1866 (1973).
21. S.T. Thornton, D.E. Gustafson, J.L.C. Ford. jr, K.S. Toth, D.C. Hensley, Phys. Rev. C **13**, 1502 (1976).
22. P.-O. Soderman, J. Blomgren, A. Ringbom, N. Olsson, L. Nilsson, J.A. Bordewijk, S. Brandenburg, G. van't Hof, M.A. Hofstee, H. van der Ploeg, S.Y. van der Werf, A. Krasznahorkay, A. Baanda, D. Chmielewska, H. Laurent, Nucl. Phys. A **587**, 55 (1995).
23. M.J. Rhoades-Brown, M. Prakash, Phys. Rev. Lett. **53**, 333 (1984); S. Santra *et al.*, Phys. Rev C **60**, 034611 (1999).
24. V.A. Ziman, A.T. Rudchik, A. Budzanowski, V.K. Chernievsky, L. Glowacka, E.I. Koshchy, S. Kliczewski, M. Makowska-Rzeszutko, A.V. Mokhnach, O.A. Momotyuk, O.A. Ponkratenko, R. Siudak, I. Skwirczynska, A. Szczurek, J. Turkiewicz, Nucl. Phys. A **624**, 459 (1997).
25. G.R. Satchler, *Direct Nuclear Reactions* (Oxford University Press, Oxford, 1983).
26. M. Conjeaud, S. Harar, E.F. Da Silveira, C. Volant, Nucl. Phys. A **250**, 182 (1975).
27. I.J. Thompson, Nucl. Phys. A **505**, 84 (1989).
28. S.V.S. Sastry, Phys. Rev. C **58**, 3753 (1998).